JACS
JOURNAL OF THE AMERICAN CHEMICAL SOCIETY

ARTICLE

pubs.acs.org/JACS

Classical Simulations with the POLIR Potential Describe the Vibrational Spectroscopy and Energetics of Hydration: Divalent Cations, from Solvation to Coordination Complex

Revati Kumar and Tom Keyes*

Department of Chemistry, Boston University, Boston, Massachusetts 02215, United States

Supporting Information

ABSTRACT: POLIR, a polarizable water potential optimized for vibrational and intermolecular spectroscopy in pure water but not optimized for solvation, is used to describe solutions of the divalent metal cations Ca^{2+}, Mg^{2+}, and Cu^{2+}. The spectral shifts in the O−H stretch region obtained from classical simulations are in agreement with experiment. The water−ion binding energies are dominated by classical electrostatics, even though the Cu^{2+} case might be considered to involve an intermediate-strength chemical bond. Three-body energies of the ion with the first solvation shell are in agreement with ab initio calculations. Our results indicate the importance of polarization in the development of accurate, transferable, force fields and the power of classical methods when it is carefully included.

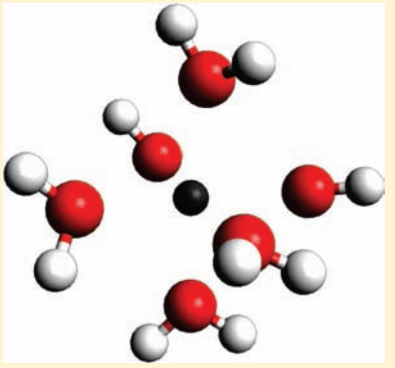

1. INTRODUCTION

Extensive theoretical and experimental studies have been performed on liquid water and on aqueous solutions.[1−6] Classical statistical mechanics requires a force field. The simplest are effective two-body potentials such as SPCE/E[7] and the TIP[8] family. However, a number of potentials have been developed to incorporate many-body interactions, which are unquestionably important, mostly via dipole polarizability.[9−17] Rigid models can describe rotation and translation only. However, the flexible-TTM family combines a polarizable force field with a highly accurate intramolecular potential in an attempt to describe vibrational spectroscopic properties.[9,14,15]

POLIR,[16] a POLarizable water potential optimized for IR, was designed to provide the best possible classical description of vibrational and intermolecular spectroscopy. The idea is that a very careful treatment of polarization is essential to describe the response of molecular vibrations to a condensed-phase environment.[9,14−16] Conversely, it was argued that optimizing the potential for spectroscopy is a natural way to optimize the treatment of polarization, which is essential for all water properties.

POLIR yields an excellent description of the frequencies and absolute absorption intensities of liquid water, water clusters, and ice, including combination bands. It also performs well on thermodynamics and kinetics, even though it has not been optimized for, e.g., $g(r)$, as is routinely done with empirical potentials.

Polarization provides the many-body interactions that are necessary for the transferability of a potential among diverse environments, but the transferability of a given potential can be established only with detailed testing. While the results are encouraging so far, POLIR has yet to be applied to several environments central to physical chemistry, notably the ionic solvation shell. In the following, using classical simulations, we present the spectroscopy, structure, and energetics of POLIR water solvating Ca^{2+}, Mg^{2+}, and Cu^{2+}.

The alkaline earth ions such as Ca^{2+} and Mg^{2+} play important roles in biology. For example, Ca^{2+} is necessary for physiological functions such as muscle contraction, whereas Mg^{2+} is a constituent of many enzymes.[18] Transition metal ions such as Cu^{2+} are vital for the function of biochemical systems.

The behavior of the ions depends upon their hydration, and vibrational spectroscopy provides a probe of the waters in the solvation shell. Interestingly, while most aqueous solutions of cations show a blue-shifted component in the O−H stretch region compared to neat water, cations with high charge to radius ratios such as Mg^{2+}, Cu^{2+}, Al^{3+}, etc. show red-shifted components.[19,20]

Although the spectroscopy of monovalent alkali metal ion solutions has been studied using various simulation techniques,[21,22] the spectra of waters solvating divalent metal ions have received less attention. However, the structure and dynamics of aqueous solutions of divalent cations have been simulated using a wide range of nonpolarizable and polarizable force fields, as well as ab initio molecular dynamics.[23−30]

The small, doubly charged ions have the strongest interactions with their hydrating waters and hence represent the most

Received: February 23, 2011
Published: May 05, 2011

dx.doi.org/10.1021/ja201695d | J. Am. Chem. Soc. 2011, 133, 9441–9450

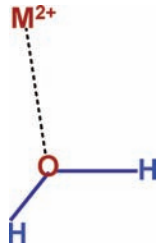

Figure 1. Water−ion dimer system.

challenging tests of POLIR. Additionally, there is a test of the classical description itself. The solute−solvent interaction increases from Ca^{2+} to Mg^{2+} to Cu^{2+}, and there is a progression from ordinary solvation to the formation of a coordination complex, which might be considered to involve chemical bonds of intermediate strength. We have previously argued that a careful treatment of short-ranged electrostatics, including polarization, yields "electrostatic bonds", allowing classical mechanics to treat some interactions and phenomena that might be thought to require quantum mechanics, and here we further explore this idea.[31]

Our primary finding is that classical simulations with POLIR and polarizable ion−water potentials constructed in the same spirit reproduce the essential experimental findings on the spectra of water in the solvation shell and reveal the mechanism of the observed frequency shifts. The structure, dynamics, and energetics of the solvated waters are also obtained, in good agreement with experiment and with other simulations.[24,25,27] For Mg^{2+} and even more so with Cu^{2+}, the water−ion interaction does indeed begin to exhibit properties of a chemical bond, and the binding energy is electrostatic energy.

2. METHODOLOGY

We begin with a brief description of POLIR; more details may be found in ref 1. The atoms are assigned charges, permanent dipoles, and induced dipoles via isotropic polarizabilities; the total atom dipole is the sum of the permanent and induced contributions, and the molecular dipole is the sum of the atom dipoles plus the "charge dipole". The charge on each atom is a function of the intramolecular O−H distances. The monomer energy is given by the highly accurate Partridge−Schwenke (PS) surface.[32] The total energy, U, is as follows:

$$U = U_{cc} + U_{cd} + U_{dd} + U_{id-id} + U_{pair} + U_{PS} - U^0_{mon} \qquad (1)$$

Here, U_{cc}, U_{cd}, and U_{dd} denote the charge−charge, charge−total dipole, and total dipole−total dipole interactions, U_{id-id} is the self-energy of the induced dipoles, and U_{pair} is the van der Waal's energy.

All inter- and intramolecular interactions are allowed, including those between bonded atoms, and hence the zero-field monomer electrostatic energy, summed over all molecules, U^0_{mon}, is removed to prevent double counting with the PS (U_{PS}) energies. Thus, a monomer in zero external field is described exactly by the PS potential, but a finite field changes the intramolecular potential and the vibrational frequencies. The Thole[33] "smeared charge" scheme is used to damp the charge−charge, charge−dipole, and dipole−dipole interactions at short-range.

2.1. Ion−Water Potentials. The Mg^{2+} and Ca^{2+} ions were assigned charges of +2 and polarizabilities taken from the literature (0.1 and 0.55 Å^3, respectively).[27] van der Waals interactions of form $((A_{16})/(r_{iO}^{16}) + (A_{14})/(r_{iO}^{14}) + (A_{12})/(r_{iO}^{12}) + (A_6)/(r_{iO}^{6}))$ were included, where r_{iO} is the ion-(water oxygen) distance. As in the POLIR potential, the power of r_{iO} in the exponentials involving the Thole damping term was 4, following Burnham's recent work.[15]

Table 1. Parameters for the Ca^{2+}−Water Interaction[a]

parameter	value
A_{16} (kcal/mol) Å ^{16}	1.0887×10^7
A_{14} (kcal/mol) Å ^{14}	-9.4245×10^6
A_{12} (kcal/mol) Å ^{12}	2.1042×10^6
A_6 (kcal/mol) Å ^{6}	−2082.49
a_{CC}	0.5
a_{CD}	0.15
a_{DD}	0.3
$\alpha_{Ca^{2+}}$ Å ^{3}	0.55

[a] The Thole damping constants for the dipole−dipole, charge-dipole, and charge−charge interactions are denoted a_{DD}, a_{CD}, and a_{CC}, respectively.

Table 2. Parameters for the Mg^{2+}−Water Interaction[a]

parameter	value
A_{16} (kcal/mol) Å ^{16}	80.2134×10^4
A_{14} (kcal/mol) Å ^{14}	-91.9328×10^4
A_{12} (kcal/mol) Å ^{12}	28.1798×10^4
A_6 (kcal/mol) Å ^{6}	−1535.63
a_{CD}	0.01
a_{DD}	0.001
a_{CC}	0.5
$\alpha_{Mg^{2+}}$ Å ^{3}	0.1

[a] The Thole damping constants for the dipole−dipole, charge-dipole, and charge−charge interactions are denoted a_{DD}, a_{CD}, and a_{CC}, respectively.

Table 3. Parameters for the Cu^{2+}−Water Interaction[a]

parameter	value
A_{16} (kcal/mol) Å ^{16}	2.42709×10^6
A_{14} (kcal/mol) Å ^{14}	-2.31326×10^6
A_{12} (kcal/mol) Å ^{12}	6.02506×10^5
A_6 (kcal/mol) Å ^{6}	−3404.29
a_{CC}	0.5
a_{CD}	0.05
a_{DD}	0.3
$\alpha_{Cu^{2+}}$ Å ^{3}	0.55

[a] The Thole damping constants for the dipole−dipole, charge-dipole, and charge−charge interactions are denoted a_{DD}, a_{CD}, and a_{CC}, respectively.

Electronic structure calculations on the ion−water dimers were performed (see Figure 1) to obtain the global minima. We then scanned the ab initio energy as a function of r_{iO} about the global minimum and the van der Waals "A" parameters, and the decay constants in the Thole damping exponentials for charge-dipole (a_{CD}) and dipole−dipole (a_{DD}) terms, were adjusted to reproduce the results (Tables 1 and 2).

We modeled the Cu^{2+}−water interaction in a similar fashion, and the polarizability of Cu^{2+} was taken from an ab initio calculation. Table 3 lists the values of all the parameters.

The fits constitute an important test of the electrostatic bond idea. If it is to describe the ion−water interaction, the van der Waals contribution must be primarily repulsive, with the attractive potential minimum arising from electrostatics. Then, as in textbook ionic bonding, fixing the pair separation at the true value and evaluating the electrostatic energy

yields the binding energy. The difference from ionic bonding is that the electrostatic energy is not approximated as the Coulomb energy, enabling an extension of the classical binding picture to systems that would otherwise require a quantal treatment.

No attempt was made to control the relative contributions of the van der Waals potential and the electrostatic potential in the fits. Nevertheless, the proposed electrostatic bond scenario was indeed confirmed. The van der Waals potential for Ca^{2+} is purely repulsive, and for Mg^{2+} and Cu^{2+} it has a weak attraction, providing only a few percent of the binding energy.

2.2. IR Spectroscopy and Rotational Dynamics. The classical IR spectrum is proportional to the Fourier transform, denoted $C(\omega)$, of the time autocorrelation function (TCF), $C(t)$, of the total dipole moment of the simulation box, $\boldsymbol{M}(t)$. The charges, permanent dipoles, and induced dipoles on the water molecules, plus the induced dipole on the ions, all contribute to $\boldsymbol{M}$. The classical TCF is corrected using the harmonic quantum intensity correction, $Q(\omega)$. The final expression for the absolute intensity is

$$I(\omega) = 4\frac{\pi^2\omega}{3cV\hbar}(1 - e^{-\beta\hbar\omega})Q(\omega)C(\omega) \quad (2)$$

where V is the volume of the box.

We employ the Berens−Wilson anharmonic quantum frequency correction,[34] expressing the difference between the frequency at the bottom of the potential well, seen in classical simulations, and the quantal $0 \rightarrow 1$ transition frequency. The PS monomer potential acquires a 184 cm^{-1} red-shift of the OH stretching band, and a 187 cm^{-1} shift was previously found[16] with an effective bulk liquid potential, indicating that the shift is quite constant upon condensation. Now we need to determine the shift for water strongly interacting with an ion.

To do so, we first perform an ab initio scan of the energy of the isolated water monomer as a function of one of the O−H bond lengths. The potential energy curve was fit to a Morse oscillator, $U = D(1 - e^{a(r-r_e)})^2$, where the harmonic frequency, γ_0, obeys

$$\gamma_0^2 = \frac{a^2}{4\pi^2}\frac{2D}{\mu} \quad (3)$$

where μ is the reduced mass; the anharmonicity correction is $((h\gamma_0)^2)/(2D)$. Repeating the procedure for the ion−water dimer, varying an O−H bond length while keeping the other O−H and the ion−O distance fixed, yields a self-consistent estimate of the O−H anharmonicity correction for water in the first solvation shell relative to that of the monomer.

To examine the contributions to the spectra, in particular in the O−H stretch region, from water molecules in different environments, we calculated the spectra resulting from waters in different solvation shells around the ion. For example, the spectrum arising from the first solvation shell was calculated as follows. On each MD time step, waters were defined as belonging to the first shell if the ion−O distance was inside the first minimum of the ion−O radial distribution function. This shell can vary during the simulation, but typically a divalent cation is surrounded by a distorted octahedral arrangement of waters. The autocorrelation function of the total dipole moment of the first-shell waters, permanent plus induced, is used to determine the spectrum. Similarly, a range of ion−O distances defines the second shell, etc. Since the induced dipoles are created by local fields from all the species in the box, the result is not a property of the indicated shell only. Nonetheless, these spectra are useful in identifying the species that give rise to different signatures in the IR spectra.

Additional information about the dynamics of the waters in the different shells, specifically the rotational dynamics, can be determined from the TCF of any molecule-fixed unit vector, $\hat{b}$:

$$C_{rot}(t) = \langle P_2(\hat{b}(t)\cdot\hat{b}(0))\rangle \quad (4)$$

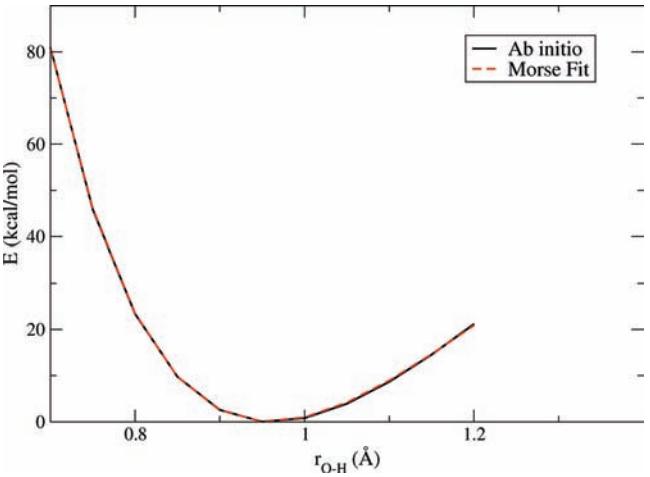

Figure 2. Ab initio scan of an O−H bond in the isolated water monomer along with the fit to a Morse potential.

where $P_2(x)$ is the second Legendre polynomial. The vector that we use is the unit vector along the O−H bond and the long time decay of the corresponding TCF corresponds to the rotational anisotropy decay measured in ultrafast IR spectroscopy.[35,36] Once again, TCFs of water molecules in different solvation shells were calculated.

2.3. Computational Details. Molecular dynamics simulations were carried out in the NVE ensemble using our in-house code with a cubic simulation box of length 15.64 Å, containing 127 water molecules and a single ion. The long-range electrostatic interactions were treated using Ewald sums.[37] The system was initially equilibrated in the NVT ensemble at 300 K.[38]

The ab initio calculations were performed at the MP2 level of theory using Gaussian03[39] with the aug-cc-pVTZ basis set for the Mg^{2+}−water system and the 6-31G(2d,2p) basis set for the Ca^{2+}−water system. The Cu^{2+}−water system was studied using the UB3LYP level of theory, with the 6-31G(2d,2p) basis set, which is computationally less expensive than the MP2 method. The polarizability of the Cu^{2+} ion was also computed with this basis set and level of theory.

3. RESULTS AND DISCUSSION

3.1. Anharmonicity Correction. The scan of the water monomer O−H stretch is shown in Figure 2. Fitting to a Morse potential yields $D = 107.83$ kcal/mol, $a = 2.40787$ $Å^{-1}$, $r_e = 0.959$ Å, and thence a harmonic frequency of 3957 cm^{-1} and an anharmonicity correction of 208 cm^{-1}. The scan for the Mg^{2+}−water dimer, along with the Morse potential fit, is shown in Figure 3: now $D = 92.429$ kcal/mol, $a = 2.447$ $Å^{-1}$, $r_e = 0.975$ Å, the harmonic frequency is 3723 cm^{-1}, and the anharmonicity correction is 214 cm^{-1}. A similar procedure for the calcium ion−water system (using the 6-31G(2d,2p) basis set) gives an anharmonicity correction of 224 cm^{-1}, while the same basis set for the isolated water molecule gives an anharmonicity shift of around 214 cm^{-1}.

The change in the anharmonicity correction between the isolated monomer and the ion−water dimer is small enough to be neglected. Note that the PS potential was parametrized to a much higher level of theory and basis set than the current calculations, resulting in a slightly different value of 184 cm^{-1}. The point of this exercise is to show that, within a given approximation, the ion does not significantly influence the anharmonicity correction, and hence we continue to use the

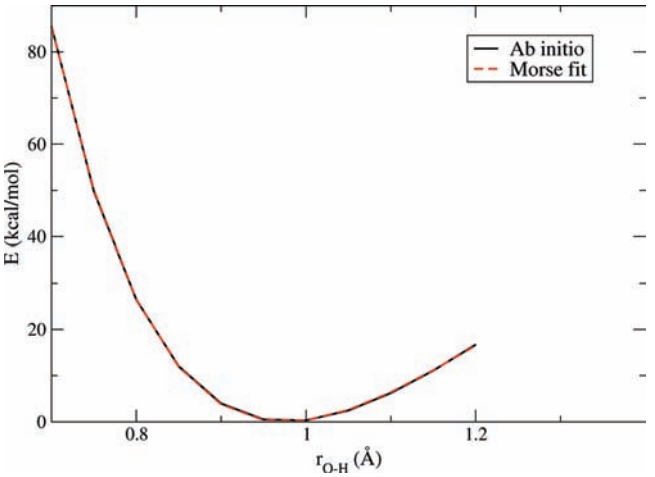

Figure 3. Ab initio scan of an O−H bond for the Mg^{2+}−water dimer along with the fit to a Morse potential.

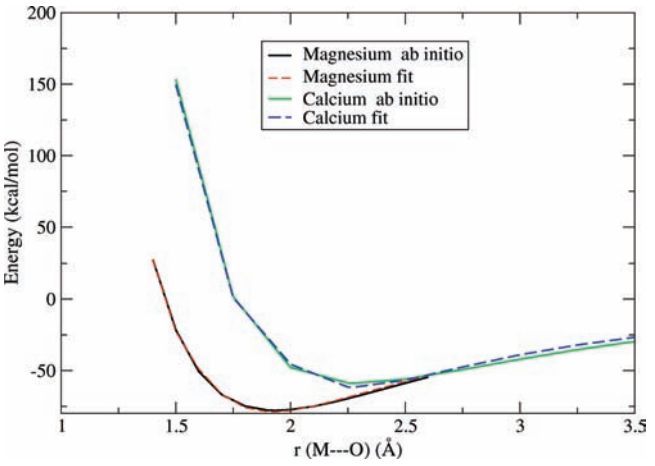

Figure 4. Dimer energy of the Ca^{2+}−water and Mg^{2+}−water systems.

PS value 184 cm^{-1} for the ion−water solutions. The constancy of the correction is important for the utility of the classical approach: the quantal frequency shifts are approximately equal to the classical shifts, and the correction need not be recalculated for each environment.

3.2. Alkaline Earth Ions Ca^{2+} and Mg^{2+}. *Structure of the Solvation Shell.* Figure 4 shows the ab initio ion−water potentials for both Ca^{2+} and Mg^{2+}. Clearly, Mg^{2+} binds more strongly to water than does Ca^{2+}. The parameters for the Mg^{2+}−water and Ca^{2+}−water potentials were determined by fitting to these results and are listed in Tables 2 and 1, respectively. Although the potentials are fit to a dimer system, polarization ensures that they include many-body interactions in solution, and the results of our simulations are discussed below.

The ion−(water O) radial distribution functions, Figure 5, reveal that the first minimum for Mg^{2+} is at at a smaller ion−O atom distance than in the case of Ca^{2+}. This is not surprising, as the minimum in the Mg^{2+}−water pair potential is also at a smaller distance, and with a greater binding energy. The first peak is at $r = 2.05$ Å for Mg^{2+} and at $r = 2.43$ Å for Ca^{2+}. These results are in agreement with simulations performed using the AMOEBA[10] water model as well as with ab initio based simulations and experimental results.[27,28,40−43]

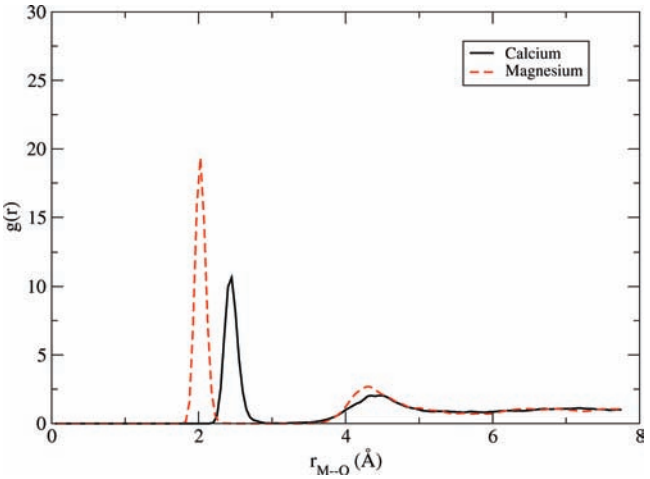

Figure 5. Oxygen−metal ion radial distribution functions.

Table 4. Distribution of Donor and Acceptor Hydrogen Bonds in the First Solvation Shell around the Divalent Calcium Ion

type	no. bonded to 1st shell	no. bonded to 2nd shell	total
donor	0.02	1.97	1.99
acceptor	0.02	0.30	0.32

Table 5. Distribution of Donor and Acceptor Hydrogen Bonds in the First Solvation Shell around the Divalent Magnesium Ion

type	no. bonded to 1st shell	no. bonded to 2nd shell	total
donor	0.03	2.00	2.03
acceptor	0.03	0.21	0.24

We calculate the number of water molecules coordinated to the ions, i.e., in the first solvation shell, by using the first minima (2.35 Å for Mg^{2+} and 3.2 Å for Ca^{2+}) in the ion−O distribution functions to define the outer boundary of the shell. For magnesium the coordination is found to be exactly 6, while for calcium it varied between 6 and 7 with an average value of 6.2. For Mg^{2+} no exchanges were observed between water molecules in the first and second shell during the simulation run, whereas for the Ca^{2+}, on average, one exchange occurs every 2.3 ps, in keeping with the exchange rate of 0.4/ps observed by Lightstone et al. for their ab initio simulation of divalent calcium ion in water.[25]

We also analyzed the hydrogen bonding of water molecules in different environments. Our primary definition is that two water molecules are hydrogen-bonded if the distance between the H-atom of one (the donor) is within 2.5 Å of the O atom of the other (the acceptor),[44] and the angle, denoted α, is then the supplement of the angle O−H···O. Alternatively, Madan et al.[45,46] introduced an angle, β, to be discussed below in the interpretation of the IR spectra(Figure 6): for every pair of water molecules one calculates the O···O distance. If the distance is less than 3.4 Å, β is the smallest of the four O−O−H angles.

The average number of hydrogen bonds per water molecule in the first solvation shell of magnesium is 2.27, and for calcium it is 2.31. For both ions, the hydrogen atoms of the first-shell waters

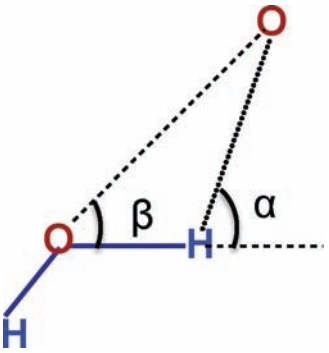

Figure 6. Definition of two possible hydrogen bond angles, α and β.

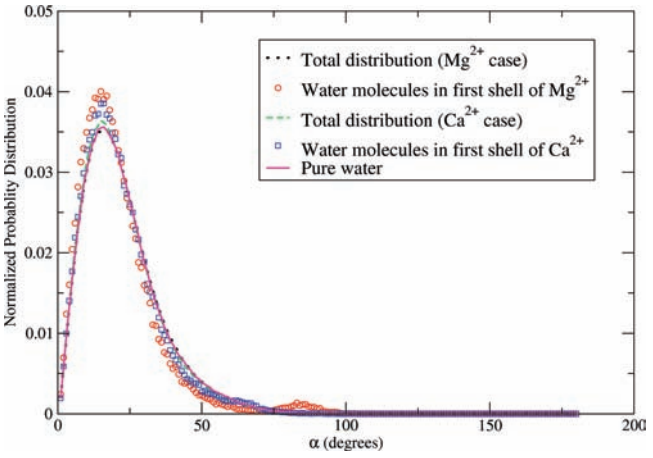

Figure 7. Distribution of the hydrogen bond angle, α, in neat water, calcium ion solution, and magnesium ion solution, along with the distribution in the first solvation shell for each ion.

almost always participate in hydrogen bonding, whereas few first-shell O atoms do so. Tables 4 and 5 list the distribution of hydrogen bonds made by first-shell waters, intrashell and to the second solvation shell, for Ca^{2+} and Mg^{2+}, respectively. From the tables it is clear that although the fraction of first-shell O atoms participating in hydrogen bonding is very small for both ions, it is on average smaller for the magnesium case.

The normalized distributions of the angle, α, in neat water, in Mg^{2+} and Ca^{2+} solutions, and in their respective first shells, are shown in Figure 7. The first-shell distribution for Mg^{2+} shows a peak at large angles, which is not seen in neat water. A similar peak, although much smaller and at a relatively smaller angle, is seen for Ca^{2+}.

The first solvation shell of water molecules around Mg^{2+} is extremely crowded, with oxygens forced to be quite close to each other (approximately 2.8 Å for the nearest neighbor O−O distance). This results in a small fraction of distorted hydrogen bonds with large angles. At the same time one sees an increase in peak height in the nondistorted region.

The tightly packed waters hydrating Mg^{2+} show additional angular distortions, which can be seen with the alternative hydrogen bond angle, β. In Figure 8 we plot its normalized distribution for neat water, and for first-shell water around Mg^{2+} and Ca^{2+}. All three show a peak at ∼10°. In the large angle region, Mg^{2+} shows two distinct peaks, one near the neat water peak and an additional peak at even larger angles. This second

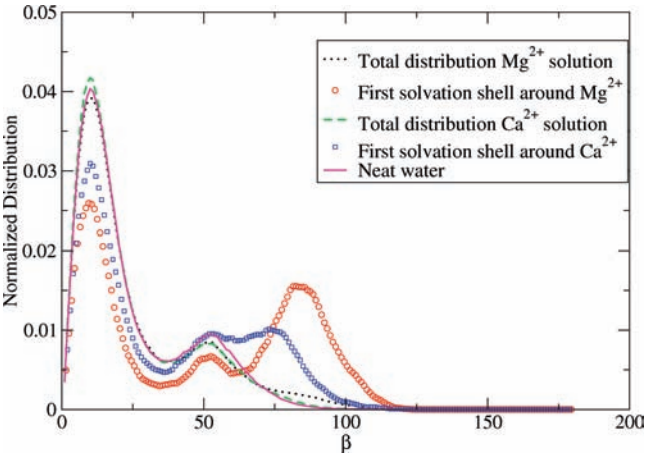

Figure 8. Distribution of the alternative hydrogen bond angle β in neat water, calcium ion solution, and magnesium ion solution, along with the distribution in the first solvation shell.

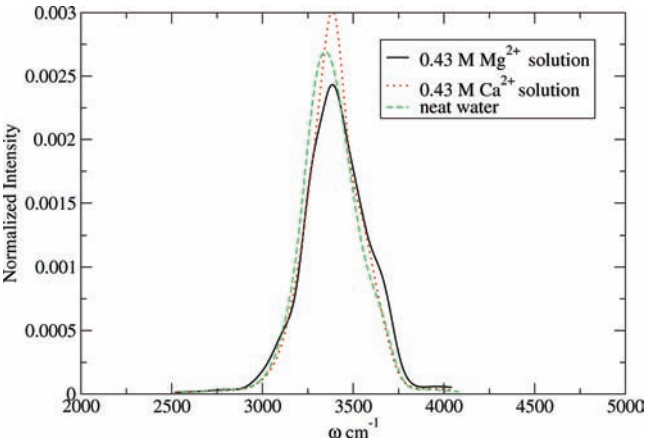

Figure 9. Normalized IR spectra in the O−H stretch region for neat water, magnesium ion solution, and calcium ion solution.

peak arises from first-shell waters that are very close to each other without a hydrogen bond (i.e., H···O distance less than 2.5 Å) between them. It should be pointed out that in neat water an O···O distance of less than 3.5 Å always corresponds to a hydrogen bond, which clearly need not be the case in the first solvation shell of Mg^{2+}.

Calcium, on the other hand, shows a much smaller second peak in the large-β region and is closer to the neat water case. These results are consistent with a picture of a highly compact, tight solvation shell in the case of Mg^{2+}, whereas the Ca^{2+} shell is larger and looser.

Another angle of interest is the intramolecular H−O−H angle, which requires a flexible potential for discussion. One of the strengths of POLIR is that, with classical electrostatics only, it correctly predicts the increase of this angle upon condensation, from 104° to 107°.[47] In the first solvation shell around Mg^{2+}, the averaged angle in our simulations decreases to 100°! It would be very interesting if the prediction of considerably more bent waters in the first shell could be verified by experiment.

IR Spectra of Hydrating Waters. IR spectra were calculated with eq 2. The normalized spectra in the O−H stretch region for pure water, water−magnesium ion, and water−calcium ion are

dx.doi.org/10.1021/ja201695d |*J. Am. Chem. Soc.* 2011, 133, 9441–9450

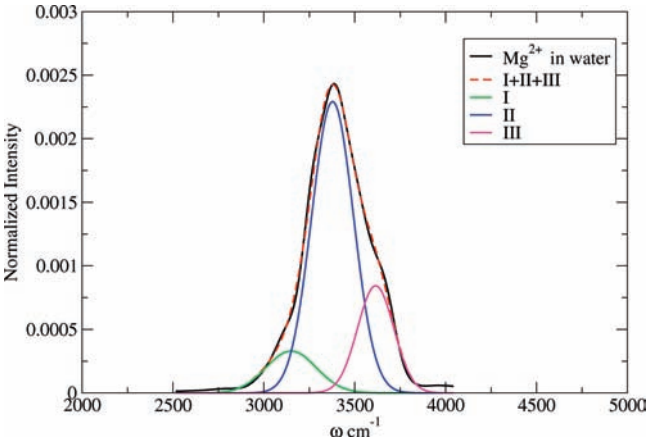

Figure 10. Normalized IR spectra in the O−H stretch region for the magnesium ion solution, along with the fit to three Gaussians.

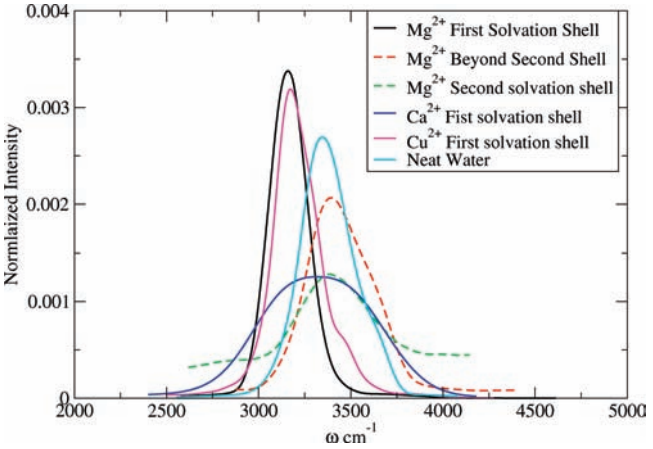

Figure 11. Normalized IR spectra in the O−H stretch region for the water molecules in the first, second, and outer solvation shells of the magnesium ion, and in the first shell around the copper and calcium ions, along with the spectrum for neat water.

plotted in Figure 9. For solvated Mg^{2+} we see two shoulders, one on the red side and the other on the blue side of the peak. Solvated Ca^{2+} shows a blue shoulder only, which is narrower than in the magnesium case. The Mg^{2+} spectrum may be almost perfectly represented, Figure 10, by a sum of three gaussians: one centered at ∼3200 cm^{-1}, a second at ∼3380 cm^{-1}, and a third at ∼3600 cm^{-1}.

It has been shown experimentally, by Stangret et al. and Lindgren et al., that cations with high charge to radius ratios such as Mg^{2+} produce a red-shifted component in the OD stretch of HOD in liquid H_2O, with respect to the liquid without ions.[20,48] They attributed this shift to the HOD molecules in the first solvation shell.

To test our classical theory against the experimental findings, we calculated the spectra of the ions in each solvation shell, as mentioned earlier in Methodology. The definitions of the shells were based on the Mg^{2+}−O radial distribution function. The first minimum at 2.35 Å is taken to define the first shell, water molecules between 2.35 and 5.5 Å from the ion are in the second shell, and those further away than 5.5 Å were considered to be third shell and beyond. The spectrum of the first-shell waters is

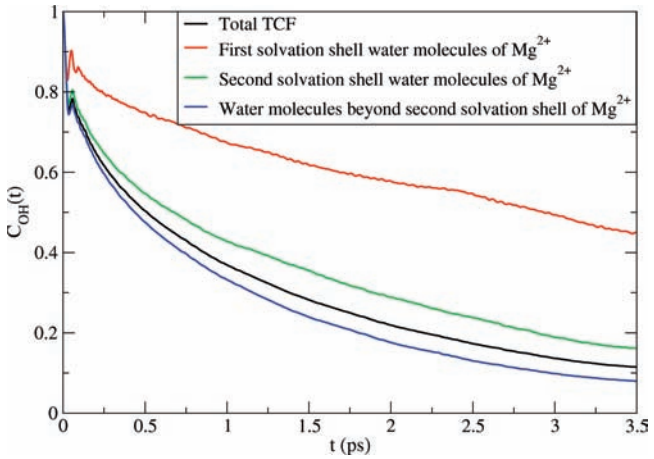

Figure 12. Rotational time correlation function (using the O−H vector) for the magnesium ion solution, along with the components from the first, second, and remaining solvation shells.

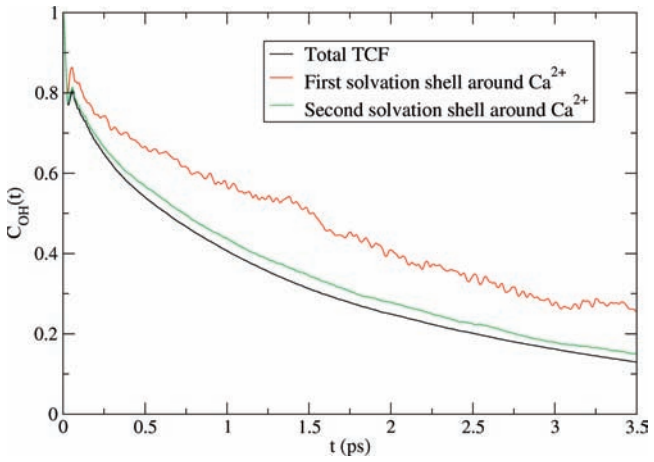

Figure 13. Rotational time correlation function (using the O−H vector) for the calcium ion solution, along with the components from the first, second, and remaining solvation shells.

clearly red-shifted to ∼3200 cm^{-1}, as seen in Figure 11, which is in keeping with the experimental observations of Stangret et al. By contrast, the first-shell spectrum for Ca^{2+}, Figure 11, shows a broad distribution which peaks near the bulk water peak.

In sum, if care is taken with polarizable electrostatics, the classical dipole correlation describes the spectra of water hydrating Mg^{2+} and Ca^{2+}.

Molecular Reorientation in the Solvation Shell. Turning to rotational dynamics, the TCF of the O−H vector is plotted in Figure 12 for Mg^{2+} solution. We have also calculated the separate contributions of water molecules in the first, second, and outermost solvation shells. The first-shell waters show very slow rotational dynamics compared to the total TCF. The second-shell waters are faster, and the waters beyond the second shell are fastest. A similar calculation for Ca^{2+} also reveals (Figure 13) slow reorientation in the first shell, but not as slow as in the case of Mg^{2+}. These results are as expected in view of the above discussion of the tightness of binding in the respective shells.

Our findings on the reorientational dynamics of hydrating waters are in keeping with the experimental results of Bakker

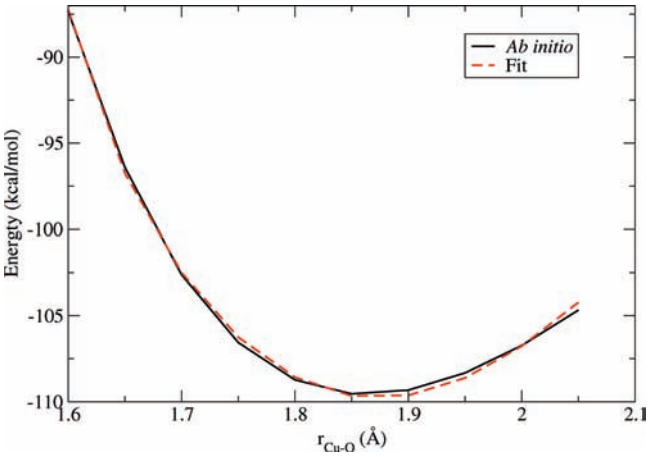

Figure 14. Dimer energy of the Cu^{2+}—water system.

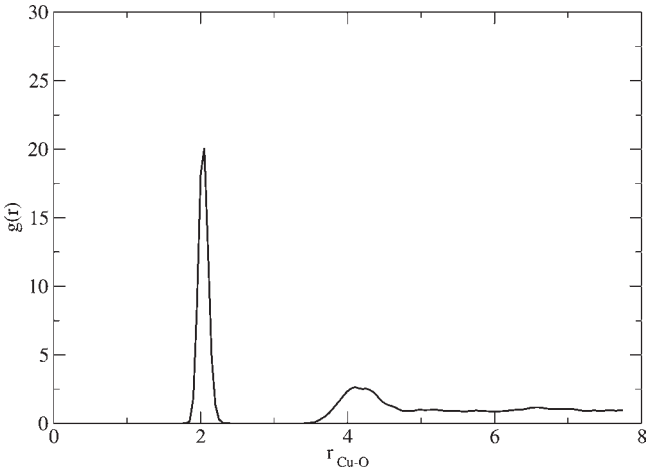

Figure 15. Oxygen—Cu^{2+} radial distribution function.

et al. on chloride.[49] They attempted to selectively probe distinct environments with two-dimensional IR. Waters beyond the first solvation shell were found to exhibit essentially bulk behavior, with a decay time of ~2 ps, which is similar to our results (2.2 ps). First-shell waters were significantly slower, ~7.6 ps, and for Mg^{2+} we find ~6.5 ps.

3.3. The Case of Cu^{2+}. Our success with the alkaline earth ions led us to explore aqueous solutions of an important transition metal ion, Cu^{2+}. Copper ions are known to form hexa-coordinated complexes with a number of ligands such as chloride, per-chlorate, etc. These complexes are typically Jahn-Teller[50] distorted structures. In aqueous Cu^{2+}, one may regard the first-shell waters as ligands, and the ion—water interactions as weak chemical bonds. Describing this system is thus an even greater challenge to classical theory than was posed by the alkaline earth ions.

There is some debate in the literature as to the structure (octahedral, distorted octahedral, square planar, etc.) of the solvation shell, or alternatively of the water ligands, around Cu^{2+} ions.[26,51−53] Interpretation of the X-ray experiments is nontrivial, although the evidence seems to weigh against a regular octahedron. However, there is no ambiguity about the presence of a red-shifted component in the O—H stretch region of the IR spectrum.[19]

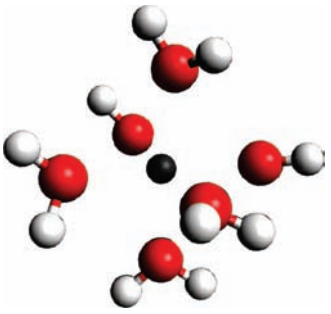

Figure 16. First solvation shell around the Cu^{2+} ion.

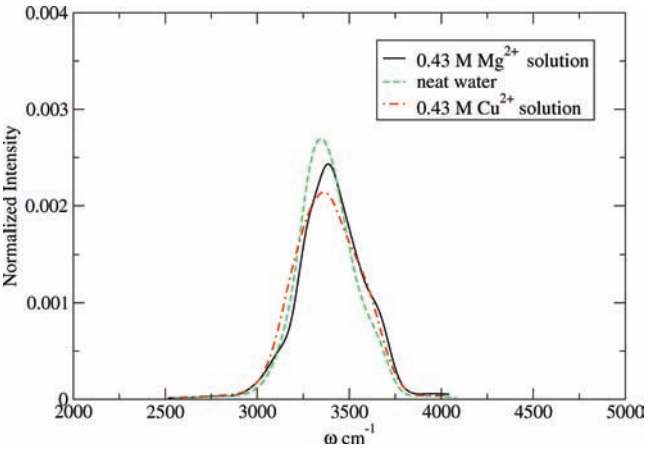

Figure 17. Normalized IR spectra in the O—H stretch region for neat water, magnesium ion solution, and copper ion solution.

Similar to the Ca^{2+} and Mg^{2+} system, we fit our parameters to the ab initio scan of the 1-dimensional PES (shown in Figure 14) of the ion—water dimers system. The Cu^{2+}—water interaction is even stronger than the Mg^{2+}—water interaction, in keeping with the idea that we are moving into an intermediate regime, between simple solvation and covalent bonding.

The Cu^{2+}—O radial distribution function is shown in Figure 15. The ion and the first solvation shell form a reasonably symmetric, hexa-coordinated octahedron (Figure 16). Similar to the magnesium case, this shell does not exchange water molecules in the available simulation time.

However, as mentioned earlier, different groups have reported different solvation structures, believed to be Jahn-Teller influenced, ranging from penta-coordinated to distorted hexa-coordinated (indicated by two close-lying peaks in the corresponding ion—water radial distribution function).[26,51−53]

The Jahn-Teller effect is quantum mechanical, so it is not surprising that we do not obtain it. With classical statistical mechanics, it seems unlikely that a pairwise additive potential could yield a Jahn-Teller structure as a free energy minimum. A many-body potential could be parametrized to reproduce Jahn-Teller. Our polarizable potential is a many-body potential, but still, apparently, favors a symmetric solvation shell. We will seek a semiclassical version of Jahn-Teller in future work.

The total IR spectrum shows a red-shifted component in the O—H stretch region (Figure 17), and the spectrum arising from the first solvation shell is red-shifted (Figure 11), just as in the case for magnesium. The red-shift arises because of the strong interaction between the copper ion and the first-shell water

dx.doi.org/10.1021/ja201695d | J. Am. Chem. Soc. 2011, 133, 9441–9450

oxygens, which weakens the O−H oscillator. Note that the interaction is changing the harmonic well-bottom frequency, not the anharmonicity correction. Again, the shift seen in classical simulation is equivalent to the quantal shift.

In sum, even though the classical theory does not yield a Jahn-Teller distortion, it captures the overall structure of the solvation shell and its lifetime, and quantitatively predicts red-shift in the spectrum of the hydrating waters.

Coordination Energy. A primary focus of our work is to establish and exploit the importance of polarization. As this has already been done for pure POLIR water, we now seek to investigate only quantities that involve a direct interaction with the Cu^{2+}. To this end we define a binding energy, or coordination energy, E^{c}_{CuW6}, as the energy of the $Cu(H_2O)_6^{2+}$ complex, taken from a snapshot of the solution, minus the energy of the $(H_2O)_6$ system. This energy was found to be −468.4 kcal/mol, and was decomposed as follows.

There are six Cu^{2+}−H_2O dimers and fifteen distinct trimers, consisting of the Cu^{2+} ion and two water molecules, $Cu(H_2O)_2^{2+}$, in the complex. The three-body energy, $E^{(3)}_{CuW2}$, of a given trimer is

$$E^{(3)}_{CuW2} = E_{CuW2} - E1_{CuW} - E2_{CuW} - E_{W2} \qquad (5)$$

where $E1_{CuW}$ and $E2_{CuW}$ are the energies of the two Cu^{2+}−water dimers, and E_{W2} is the energy of the water dimer, in the trimer. Neglecting four-body and higher order terms, the sum of the six Cu^{2+}−H_2O pair energies, E_{CuW}, and the 15 three-body energies, $E^{(3)}_{CuW2}$, should be approximately equal to the coordination energy, E^{c}_{CuW6}. The total two- and three-body components were found to be −614.5 and 193.0 kcal/mol, respectively.

The three-body energy in our model is solely due to classical polarization and is clearly not negligible, but is it correct? The ab initio three-body contribution to the "coordination energy" was found to be 191.7 kcal/mol, in very close agreement with our result of 193.0 kcal/mol. Polarization is providing a remarkable reproduction of the three body energy of the Cu^{2+}−water complex, is the essential ingredient in a classical electrostatic description of aqueous Cu^{2+}. We have optimized neither POLIR nor the ion−water potential for these energies, so this result constitutes a significant test of our approach.

In the case of the magnesium ion which is less polarizable, the coordination energy is −395.0 kcal/mol, the total two-body energy is −465.0 kcal/mol, and the three-body energy is 90.0 kcal/mol.

4. DISCUSSION

We have previously demonstrated that the polarization-centric POLIR potential can reproduce the intermolecular and vibrational spectra of water clusters, liquid water, and ice: classical mechanics is adequate for spectroscopic calculations, and POLIR is transferable. We have also argued that classical electrostatics, damped at short range and including the polarization energy, can describe intermediate-strength chemical bonds as "electrostatic bonds". Here both ideas were extended to the case of cationic solvation, which presents a strongly interacting, inhomogeneous environment to test transferability, has a considerable literature on the spectroscopy of the hydrating waters, and offers the possibility of electrostatic ion−water bonds. By considering Ca^{2+}, Mg^{2+}, and Cu^{2+}, we obtain a series with increasing strength, which might be considered to vary from physical solvation for Ca^{2+} to chemical ligand binding for Cu^{2+}.

First it was necessary to develop ion−water pair potentials compatible with POLIR, by fitting ab initio results to a sum of electrostatic plus van der Waals terms. The fits were unconstrained, allowing all possible relative contributions of the two components to the dimer binding energy. However, the result was that binding is, indeed, "electrostatic": the van der Waals potential for Ca^{2+} is entirely repulsive, and for Mg^{2+} and Cu^{2+} its tiny attraction gives only a few percent of the binding energy. Given the essential hard-core repulsions, classical electrostatics can describe the ion−water binding, even in the Cu^{2+} case where it might be considered an intermediate strength ligand−(transition metal) chemical bond.

The high charge to radius ratio of the Mg^{2+} and Cu^{2+} ion has a spectroscopic signature in aqueous solution, namely, the red-shifted component of the O−H stretch in the IR spectrum, which is not seen for more weakly interacting cations such as Ca^{2+}. Thus it is an essential test of our approach that the red-shifted component be produced by some ions and not others, and the test was passed. This signature was shown to arise from the strongly bonded POLIR water molecules in the first solvation shell. The spectral shifts are perfectly well described by classical simulation, i.e., they follow the shifts of the classical vibrational frequencies, so long as polarization is accurately incorporated.

In sharp contrast, the more weakly interacting Ca^{2+} ion shows a very small blue shift, in agreement with experiment.

Madan et al. have related features in the IR spectra of water in the presence of solutes such as sodium, potassium, urea, and TMAO to the distributions of their hydrogen bond angles, β.[21,45,46] In general, stronger hydrogen bonds flatten the OH potential and shift the frequency toward the red. They argue that a hydrophobic solute simply replaces a water placed so as to produce a distorted hydrogen bond, leading to straighter bonds and a small red-shift. By contrast, the singly charged ions they consider distort the network through the ion−water potential and cause a blue-shift.

Now we extend the picture to +2 ions. First, note that, despite its charge, Ca^{2+} behaves like the singly charged ions because of its large size. The peak at ∼50−80° for first shell waters in Figure 8 is responsible for the blue shoulder.

In Mg^{2+}, it is no longer possible to explain the spectrum with hydrogen bonding alone: the strong ion−water interaction directly weakens the O−H oscillators, leading to a red-shift. It is essential for the classical approach that this shift appears in the classical frequency and not in the quantum anharmonicity correction. Here the β distribution has two strong peaks. The H-bonds of the waters giving rise to the low-angle peak reinforce the direct interaction effect, causing the distinct red shift. Similar considerations hold for Cu^{2+}.

A coordination energy was defined for the $Cu(H_2O)_6^{2+}$ complex by removing the water-only contributions. The three-body energy, entirely due to polarization, was ∼40%, and we have already discussed that the pair binding energy is almost entirely electrostatic.

A detailed analysis of the structure and dynamics of the hydrating waters of the alkaline earth ions showed that the first shell around Mg^{2+} forms a compact, long-lived complex, which can be considered a single "superion" species, $Mg(H_2O)_6^{2+}$. In the rotational dynamics of the waters in the different solvation shells of the two ions, once again the magnesium case showed the consequences of a large charge/radius ratio, much slower orientational dynamics of the first shell waters compared to the bulk. The first shell around Cu^{2+} also forms a superion and does not exchange waters in the simulation time.

5. CONCLUSION

The POLIR potential was developed to provide a classical description of the spectroscopy of water. In this paper, by combining POLIR with polarizable ion−water potentials, we have reproduced key experimental features of the vibrational spectra of solutions of divalent cations. One might well ask why a classical approach is adequate for these strongly interacting, high-frequency systems.

First, we have captured the effects of polarization that cause the change in the induced dipole moment due to the environment. In particular, POLIR is the only potential that includes the charge-dipole interaction on bonded OH atoms. When an induced dipole changes, its interaction with the charge on a bonded neighbor changes, which changes the vibrational frequency.

Although the primary calculation is of the classical dipole correlation, we emphasize that simple quantum corrections are necessary. We have included a harmonic quantum intensity correction and an anharmonic frequency correction. We were also fortunate that gas-phase ab initio calculations revealed that the same anharmonicity correction used for pure water works for water in the presence of the divalent ions. The near-constant value of the frequency correction is essential to this work. The approach would be far less appealing with a need to recalculate the shift for every system.

The success of our simulations in predicting the spectral shifts of the O−H stretch of waters solvating three different cations indicates that a high-level polarizable potential is "transferable", correctly describing the quite different response of the waters to three distinct environments. Our conclusion is that polarizable classical methods are very powerful for solvation but that nonpolarizable calculations would be highly suspect.

This work naturally suggests several future projects. A study of the thermodynamics of solvation using the POLIR potential is underway. While the vibrational IR is the topic of this paper, the dipole correlation yields the intermolecular, librational, bending, and combination bands, and these are yet to be analyzed.

The Raman spectrum is available from the total-system polarizability correlation. Recent Raman experiments performed in the Ben-Amotz group[4] on solvated halide ions show interesting trends with anion size and isotopic substitution, which are excellent targets for POLIR.

We plan a comprehensive study of the IR and Raman spectra of normal and deuterated water and additional solutes, both charged and hydrophobic. Then we will consider water in confined and biophysical environments.

■ ASSOCIATED CONTENT

Supporting Information. Z matrices for the ion−water dimer and complete ref 39. This material is available free of charge via the Internet at http://pubs.acs.org.

■ AUTHOR INFORMATION

Corresponding Author
keyes@bu.edu

■ ACKNOWLEDGMENT

Acknowledgment is made to the donors of the American Chemical Society Petroleum Research Fund and to the National Science Foundation (grant CHE 0848427) for support of this research.

■ REFERENCES

(1) Pal, S. K.; Zewail, A. H. *Chem. Rev.* **2004**, *104* (4), 2099–2124.
(2) Jungwirth, P.; Tobias, D. J. *Chem. Rev.* **2006**, *106* (4), 1259–1281.
(3) Marcus, Y. *Chem. Rev.* **2009**, *109* (3), 1346–1370.
(4) Perera, P. N.; Browder, B.; Ben-Amotz, D. *J. Phys. Chem. B* **2009**, *113* (7), 1805–1809.
(5) Bakker, H. J.; Skinner, J. L. *Chem. Rev.* **2010**, *110* (3), 1498–1517.
(6) Skinner, J. L. *Science* **2010**, *328* (5981), 985–986.
(7) Berendsen, H. J. C.; Grigera, J. R.; Straatsma, T. P. *J. Phys. Chem.* **1987**, *91*, 6269.
(8) Jorgensen, W. L.; Chandrasekhar, J.; Madura, J. D.; Impey, R. W.; Klein, M. L. *J. Chem. Phys.* **1983**, *79*, 926.
(9) Burnham, C. J.; Xantheas, S. S. *J. Chem. Phys.* **2002**, *116* (12), 5115–5124.
(10) Ren, P.; Ponder, J. *J. Phys. Chem. B* **2003**, *107*, 5933.
(11) Defusco, A.; Schofield, D. P.; Jordan, K. D. *Mol. Phys.* **2007**, *105*, 2681.
(12) Piquemal, J.-P.; Chelli, R.; Procacci, P.; Gresh, N. *J. Phys. Chem. A* **2007**, *111* (33), 8170–8176.
(13) Kumar, R.; Skinner, J. L. *J. Phys. Chem B.* **2008**, *112* (28), 8311–8318.
(14) Fanourgakis, G. S.; Xantheas, S. S. *J. Chem. Phys.* **2008**, *128* (7), 074506.
(15) Burnham, C. J.; Anick, D. J.; Mankoo, P. K.; Reiter, G. F. *J. Chem. Phys.* **2008**, *128* (15), 154519.
(16) Mankoo, P. K.; Keyes, T. *J. Chem. Phys.* 2008, *129*(3).
(17) Kumar, R.; Wang, F.-F.; Jenness, G. R.; Jordan, K. D. *J. Chem. Phys.* **2010**, *132* (1), 014309.
(18) Cowan, J. A. *The Biological Chemistry of Magnesium*; VCH Publisher Inc.: New York, 1995.
(19) Sethna, P. P.; Pinkley, L. W.; Williams, D. *J. Phys. Chem.* **1978**, *82* (6), 683–685.
(20) Stangret, J.; Gampe, T. *J. Phys. Chem. A* **2002**, *106* (21), 5393–5402.
(21) Sharp, K. A.; Madan, B.; Manas, E.; Vanderkooi, J. M. *J. Chem. Phys.* **2001**, *114* (4), 1791–1796.
(22) Lin, Y.-S.; Auer, B. M.; Skinner, J. L. *J. Chem. Phys.* **2009**, *131* (14), 144511.
(23) Guádia, G. S.; Padró, J. A.; Kalko, S. G. *J. Soln. Chem.* **1999**, *28*, 1113.
(24) Schwenk, C. F.; Loeffler, H. H.; Rode, B. M. *Chem. Phys. Lett.* **2001**, *349* (1−2), 99–103.
(25) Lightstone, F. C.; Schwegler, E.; Allesch, M.; Gygi, F.; Galli, G. *Chem. Phys. Chem* **2005**, *6*, 1439.
(26) Amira, S.; Spangberg, D.; Hermansson, K. *Phys. Chem. Chem. Phys.* **2005**, *7*, 2874.
(27) Jiao, D.; King, C.; Grossfield, A.; Darden, T. A.; Ren, P. *J. Phys. Chem. B* **2006**, *110* (37), 18553–18559.
(28) Piquemal, J.-P.; Perera, L.; Cisneros, G. A.; Ren, P.; Pedersen, L. G.; Darden, T. A. *J. Chem. Phys.* **2006**, *125* (5), 054511.
(29) Tommaso, D. D.; de Leeuw, N. H. *Phys. Chem. Chem. Phys.* **2010**, *12*, 894.
(30) Yu, H.; Whitfield, T. W.; Harder, E.; Lamoureux, G.; Vorobyov, I.; Anisimov, V. M.; MacKerell, A. D.; Roux, B. *J. Chem. Theory Comput.* **2010**, *6* (3), 774–786.
(31) Keyes, T.; Napoleon, R. L. *J. Phys. Chem. B* **2011**, *115* (3), 522–531.
(32) Partridge, H.; Schwenke, D. W. *J. Chem. Phys.* **1997**, *106* (11), 4618–4639.
(33) Thole, B. T. *Chem. Phys.* **1981**, *59* (3), 341–350.
(34) Berens, P. H.; Wilson, K. R. *J. Chem. Phys.* **1981**, *74* (9), 4872–4882.
(35) Stirnemann, G.; Laage, D. *J. Phys. Chem. Lett.* **2010**, *1* (10), 1511–1516.

(36) Lin, Y.-S.; Pieniazek, P. A.; Yang, M.; Skinner, J. L. *J. Chem. Phys.* **2010**, *132* (17), 174505.
(37) Smith, W. *CCP5 Newsletter* **1998**, *46*, 18.
(38) Allen, M. P.; Tildesley, D. J. *Computer Simulation of Liquids*; Oxford University Press, New York, 1989.
(39) Frisch, M. J. et al. *Gaussian 03, Revision C.02*; Gaussian, Inc.: Wallingford, CT, 2004.
(40) Dang, L. X.; Schenter, G. K.; Glezakou, V.-A.; Fulton, J. L. *J. Phys. Chem. B* **2006**, *110* (47), 23644–23654.
(41) Lightstone, F. C.; Schwegler, E.; Hood, R. Q.; Gygi, F.; Galli, G. *Chem. Phys. Lett.* **2001**, *343* (5−6), 549.
(42) Badyal, Y. S.; Barnes, A. C.; Cuello, G. J.; Simonson, J. M. *J. Phys. Chem. A* **2004**, *108* (52), 11819–11827.
(43) Jalilehvand, F.; Spongberg, D.; Lindqvist-Reis, P.; Hermansson, K.; Persson, I.; Sandström, M. *J. Am. Chem. Soc.* **2001**, *123* (3), 431–441.
(44) Kumar, R.; Schmidt, J. R.; Skinner, J. L. *J. Chem. Phys.* **2007**, *126* (20), 204107.
(45) Madan, B.; Sharp, K. *J. Phys. Chem.* **1996**, *100* (18), 7713–7721.
(46) Madan, B.; Sharp, K. *Biophys. Chem.* **1999**, *78* (1−2), 33.
(47) Fanourgakis, G. S.; Xantheas, S. S. *J. Chem. Phys.* **2006**, *124* (17), 174504.
(48) Kristiansson, O.; Lindgren, J. *J. Phys. Chem.* **1991**, *95* (3), 1488–1493.
(49) Omta, A. W.; Kropman, M. F.; Woutersen, S.; Bakker, H. J. *Science* **2003**, *301* (5631), 347.
(50) Berusker, I. B. *The Jahn-Teller Effect*; Cambridge University Press: Cambridge, U.K. and New York, 2006.
(51) Pasquarello, A.; Petri, I.; Salmon, P. S.; Parisel, O.; Car, R.; Toth, E.; Powell, D. H.; Fischer, H. E.; Helm, L.; Merbach, A. E. *Science* **2001**, *291* (5505), 856.
(52) Chaboy, J.; noz Páez, A. M.; Merkling, P. J.; Marco, E. S. *J. Chem. Phys.* **2006**, *124* (6), 064509.
(53) van Duin, A. C. T.; Bryantsev, V. S.; Diallo, M. S.; Goddard, W. A.; Rahaman, O.; Doren, D. J.; Raymand, D.; Hermansson, K. *J. Phys. Chem. A* **2010**, *114* (35), 9507–9514.